Supporting Information

Plant root cell-inspired interphase layer for practical aqueous zinc-iodine batteries with super-high areal capacity and long lifespan

Experimental Section

Preparation of the Zn@TOP/Carra electrode

TOP nanorods were synthesized through a previously reported method with minor modification.[1] Typically, 5 mL phosphoric acid was added into 30 mL deionized water and mixed thoroughly to obtain solution A. And 0.681 g tetrabutyl titanate was dissolved in 10 mL acetic acid to obtain solution B. Subsequently, Solution B was added dropwise to solution A under the magnetic stirring to form a clear and transparent solution, which was transferred into a 100 mL Teflon-lined stainless-steel autoclave and heated at 180 °C for 24 h. The white precipitate was obtained by centrifugation and washed with deionized water and ethanol for three times, then dried in the vacuum oven at 80 °C for 12 h.

70 wt% TOP and 30 wt% Carra (ι-Carrageenan) were mixed with deionized water as solvent at 50 °C to obtain a homogeneous slurry. Zn foil (thickness of ~100 μm) was prior polished with 2000 mesh sandpaper and cleaned with deionized water and ethanol. Then the slurry was coated onto Zn foil through the spin coating method (EZ6-S, Jiangsu LEBO Scientific Instrument Co., Ltd), and dried naturally to obtain the Zn@TOP/Carra electrode.

Characterizations

X-ray diffraction (XRD) measurements were carried out on an Empyrean diffractometer (Malvern Panalythical) equipped with the CuKα radiation. Zeta potential measurements were obtained from the Zetasizer instrument (90 Plus PALS, Brookhaven Instrument). Scanning electron microscope (SEM) and transmission

electron microscope (TEM) images were obtained using Gemini SEM500 (Zeiss) and F200X G2 (FEI Talos), respectively. Atomic force microscope (AFM) images were obtained under tapping mode on a Cypher ES (Oxford Instruments Asylum Research). Raman spectroscopy was conducted on a LabRAM HR Evolution (Horiba) with a 532 nm wavelength of laser. The in-situ optical images were acquired on CX40M metallographic microscope (NINGBO SUNNY INSTRUMENTS) with a home-made electrochemical cell. The Ultraviolet-visible spectrum (UV/Vis) was obtained by ultraviolet spectrophotometer (UV-3600i plus, SHIMADZU). 10 mL of 0.2 M KI_3 and 10 mL of 0.2 M $ZnSO_4$ solutions were added into the left and right chamers of H-type glass communication vessel sandwiched with GF or GF@TOP/Carra separtors, respectively. Every ten minutes, the solution in the right chamber was stirred and taken 200 μL for the UV-vis spectra measurement.

In situ differential electrochemical mass spectroscopy (DEMS) was obtained by assembling Zn-Zn symmetric cells in the electrochemical cell (HPR-40 DEMS, Hidden Analytical). During the charging and discharging processes at 10 mA cm^{-2}, H_2 generated from water decomposition is continuously expelled by argon (flow rate: 5 mL min^{-1}). After removing the water by passing through the cold trap, the resultant gas mixture is analyzed using a mass spectrometer. After the measurement, a standard H_2/Ar gas (H_2 content: 5 ppm, flow rate: 5 mL min^{-1}) is used to substitute resultant gas and calculated the H_2 content during cycling.

Electrochemical measurements

CR-2032 type coin cells were assembled in the air for electrochemical tests, glass

fiber filter (GF-D, Whatman) as the separator, 2.0 M $ZnSO_4$ aqueous solution as the electrolyte. Symmetrical cells were also fabricated by using two bare Zn electrodes or two Zn@TOP/Carra electrodes, respectively. For the Zn//Cu half cells, the Cu discs were coated by TOP/Carra. The high-loading iodine electrodes were prepared through a sublimation diffusion method. Firstly, the ACC (active carbon cloth) is treated with dilute HCl and dried. Next, iodine powder and ACC were mixed and sealed in a glassy reactor and then heated at 80 °C for 30 min. The real loading mass of iodine is obtained by subtracting the mass of ACC and I_2/ACC, which is controlled to be approximately 38 mg cm^{-2}. For the fabrication of zinc-iodine batteries, the high-loading iodine electrode was adopted as the cathode, and an additional carbon felt was placed between the iodine cathode and positive battery case to ensure the conductive contact and reduce the formation of polyiodides. Cyclic Voltammetry (CV) and Electrochemical impedance spectroscopy (EIS) tests were conducted by using the electrochemical workstation (760D, CHI). Electrochemical impedance spectroscopy tests were performed by Solarton1287A + 1260A (AMETEK) in Zn-Zn symmetric cells.

Theoretical calculations

Quantum chemistry (QC) calculation was performed with Gaussian09 E.01 software in this work. [2] The B3LYP-D3[3-4] functional and def2-SVP[5] basis set was used to optimize the geometry of all structures. The vibration analysis was performed at the same theoretical level to ensure that all structures are energy minima and get Gibbs free energy correction. The high-precision single-point energy

was calculated by Gaussian09 E.01 at the B3LYP-D3/def2-TZVPP[6] theoretical level. Solvent effects of water (ε = 78.4) was considered by SMD[7]solvation model. The electrostatic potential (ESP) and restrained electrostatic potential (RESP)[8] were calculated through Multiwfn[9-10] software.

Molecular dynamics (MD) simulation was performed through Gromacs2018.8[11] software to study the Zn/electrolyte interface structure at different potentials. The small molecules (carra, I_3^-, water, $ZnSO_4$) were reasonably optimized via Gaussian09 E.01[2] software with a level of B3LYP-D3[3-4] functional and def2-SVP[5] basis set before simulations. The force field parameters of Zn^{2+} ions and SPC/E[12] water model was obtained with Amber99SB[13] force field. The GAFF[14] force field parameters of sulfate ion were generated with Acpype program[15] , carra and I_3^- were generated with Sobtop software[16]. RESP atom charges were used to describe electrostatic interactions. Atomic charges of all ions were multiplied by scale factor 0.75 to correct the polarization effect of ions.

The composition of the simulation box is 2 M $ZnSO_4$ +carra, including 2508 Zn atoms, 75 carra, 120 $ZnSO_4$ and 2833 H_2O. An 6-layer slab containing 2508 Zn atoms was build in Material studio[17-18], which used as the model of [0 0 1] surface of the Zn electrode. The other composition of the simulation box is 2 M $ZnSO_4$ +carra+I_3^-, including 2508 Zn atoms, 75 carra, 40 I_3^-, 120 $ZnSO_4$ and 2833 H_2O. An 6-layer slab containing 2508 Zn atoms was build in Material studio, which used as the model of [0 0 1] surface of the Zn electrode. The boxes of $ZnSO_4$ aqueous solution were built by filling molecules randomly. The initial structures were modelled via Packing

Optimization for Molecular Dynamics Simulations (Packmol) program[19] and the periodic box was set to 10*10*10 nm^3. All the boxes were first submitted to energy minimization by using the 10000-step steepest descent method in order to avoid unreasonable contact of system. The equilibrium simulation was carried out with NPT ensemble at 298.2 K and 1 bar for 20 ns, the non-bonding cutoff radius was 1 nm and the integration step was 1 fs. The production simulation was carried out with NVT ensemble at 298.2 K for 20 ns. The RDF function and distribution of number density was calculated through Gromacs2018.8. VMD[20] software was used to visualize the systems and obtain the ion association state. Only the final 5 ns was sampled for radial distribution function (RDF) and coordination structure counting analyses. A time step of 1 fs was used for all simulations.

All first-principles calculations based on density functional theory (DFT) were conducted through the Vienna Ab Initio Simulation Package (VASP)[21]. The electronic exchange-correlation interaction along with the GGA functional in the parameterization of the Perdew Burke and Ernzerhof (PBE) pseudopotential were analyzed by the projector augmented wave (PAW) potentials[22-23].The wave function with a cut off energy of 500 eV was represented by a plane wave.The diffusion pathways and energetics of Zn^{2+} diffusion throughout the bulk of TOP were calculated through climbing image nudged elastic band (CINEB) method. Specifically, the minimum energy paths (MEP) in the CINEB procedure were initialized by linear interpolation of 5 images between the two fully relaxed end-point geometries, and each image was converged to < 10^{-5} eV per super cell for TOP, respectively.

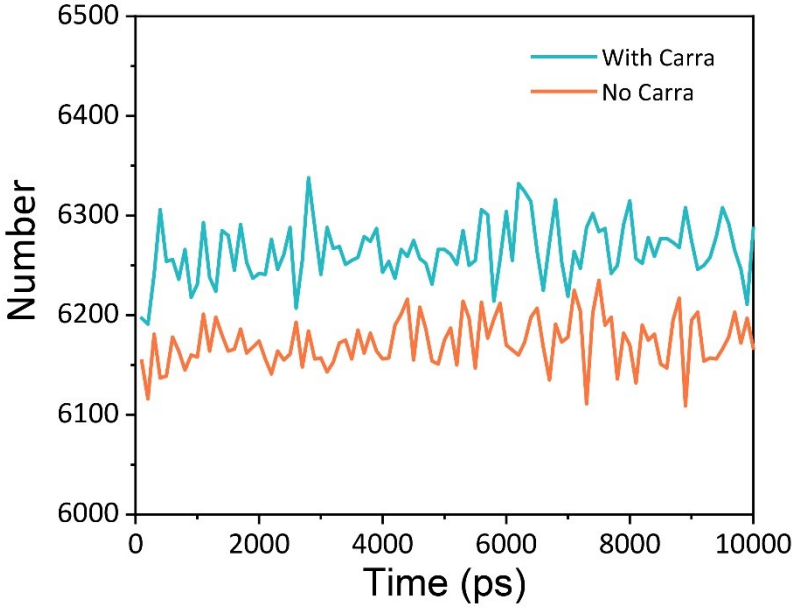

Figure S1. The statistical hydrogen bonds of Zn and Zn@Carra in MD simulations.

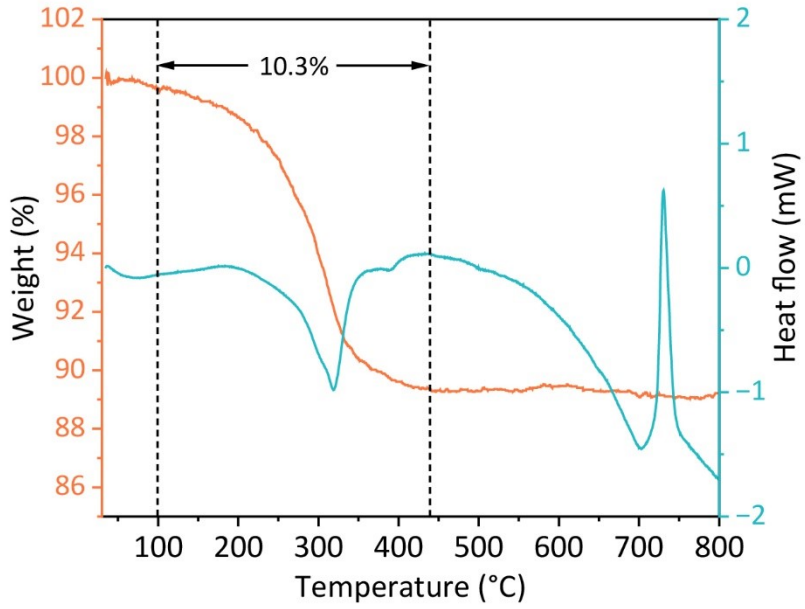

Figure S2. TGA of TOP in Ar atmosphere with the heating rate of 10 °C min^{-1}.

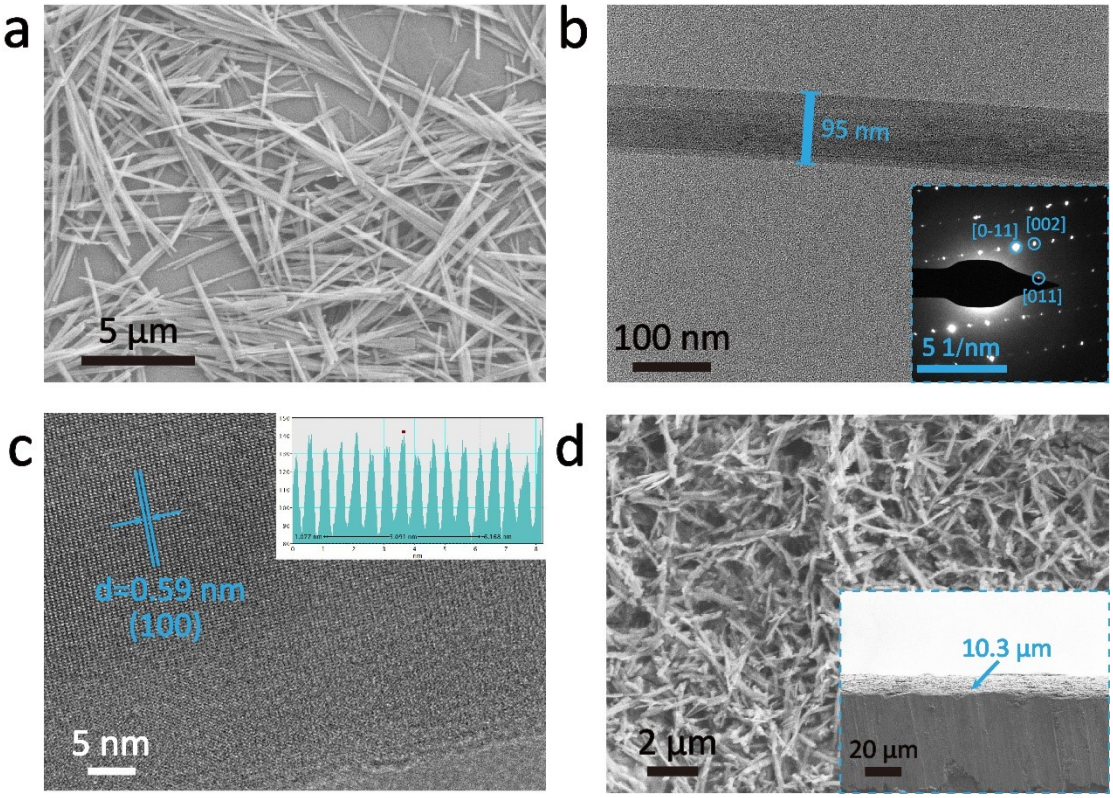

Figure S3. (a) SEM image of TOP nanorods. (b) TEM image (inset is the corresponding SAED pattern) and (c) HR-TEM image of TOP nanorods. (d) SEM image of the Zn@TOP/Carra electrode surface (inset is the cross-sectional SEM image).

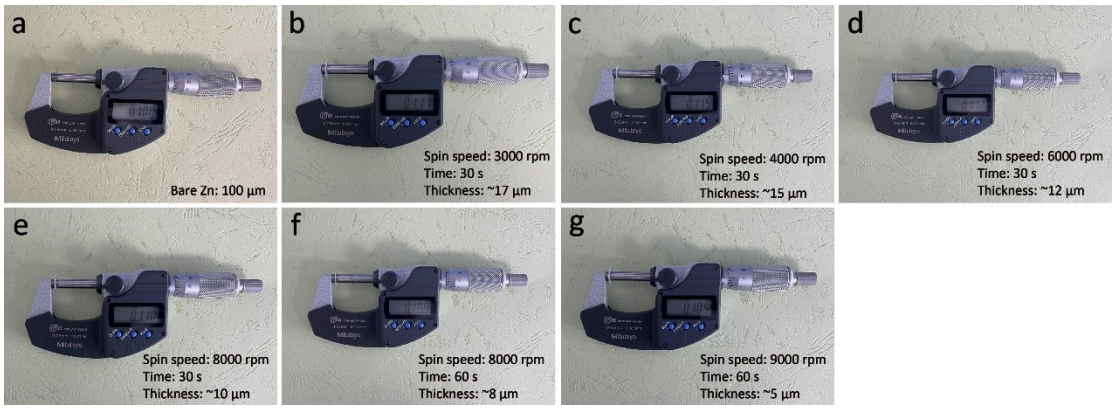

Figure S4. The thickness of (a) bare Zn and (b-g) Zn@TOP/Carra electrodes with different spin speed and rotation time.

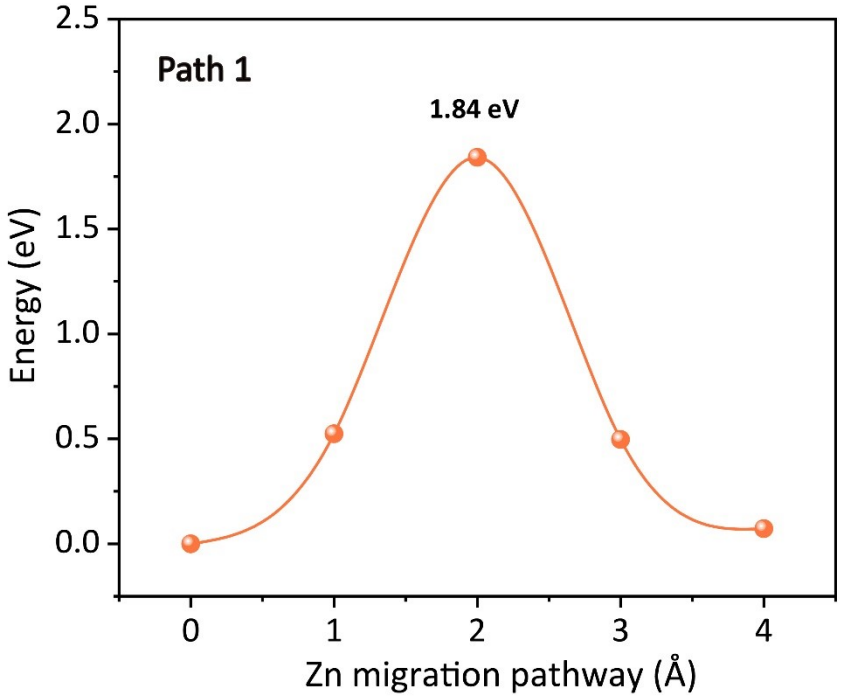

Figure S5. Zn^{2+} diffusion energy barriers in TOP through the Path 1.

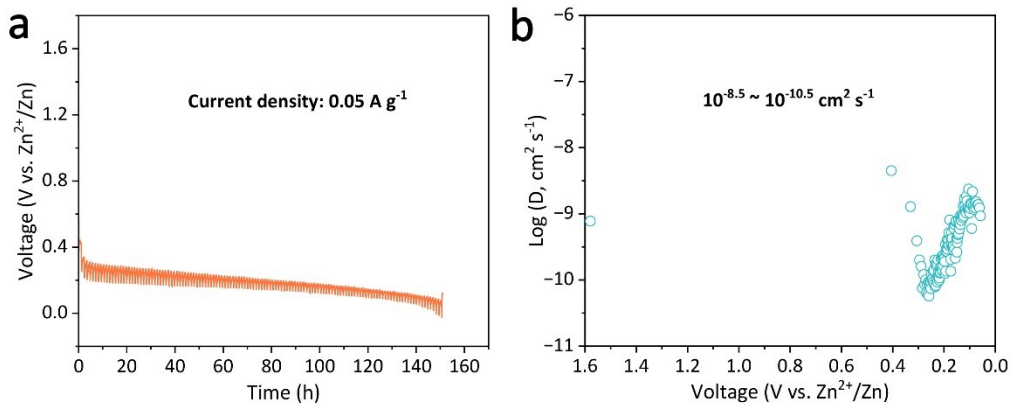

Figure S6. (a) GITT curves and (b) calculated apparent Zn^{2+} ion diffusion coefficients of TOP.

Table S1. The comparison of Zn^{2+} ion diffusion coefficients between TOP and other typical intercalating-type cathode materials.[24-27]

References	Materials	Zn^{2+} ion diffusion coefficients ($cm^2\ s^{-1}$)
Ultrafast Zinc-Ion Diffusion Ability Observed in 6.0-Nanometer Spinel Nanodots	Mn_3O_4 nanorods	2.4×10^{-10}
Unveiling the Energy Storage Mechanism of MnO2 Polymorphs for Zinc-Manganese Dioxide Batteries	MnO_2	$10^{-10.5}$~$10^{-13.5}$
Multiple Cations Nanoconfinement in Ultrathin V2O5 Nanosheets Enables Ultrafast Ion Diffusion Kinetics Toward High-performance Zinc Ion Battery	Ultrathin V_2O_5 Nanosheets	7.5×10^{-8}
Principles of interlayer-spacing regulation of layered vanadium phosphates for superior zinc-ion batteries	phenylamine (PA)-intercalated $VOPO_4 \cdot 2H_2O$	5.7×10^{-8}

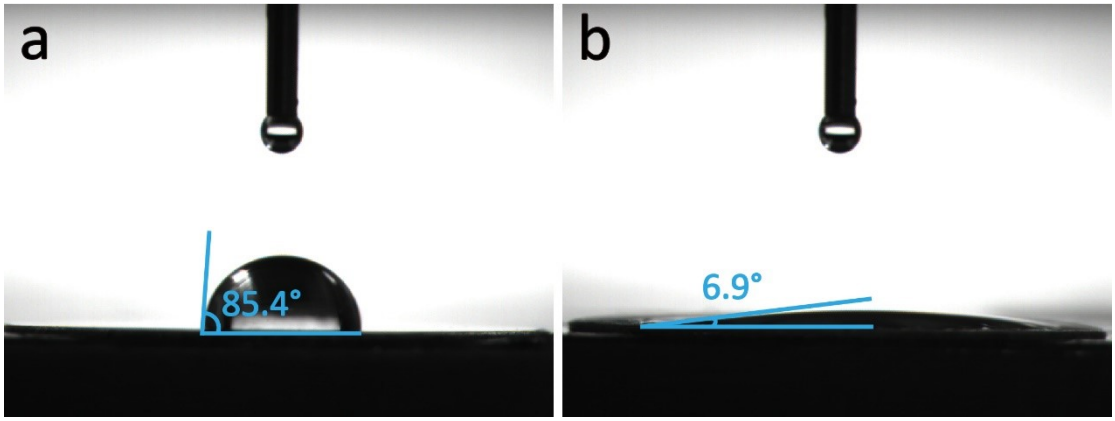

Figure S7. Contact angles of 2 M $ZnSO_4$ electrolyte (a) on Zn and (b) Zn@TOP/Carra electrodes.

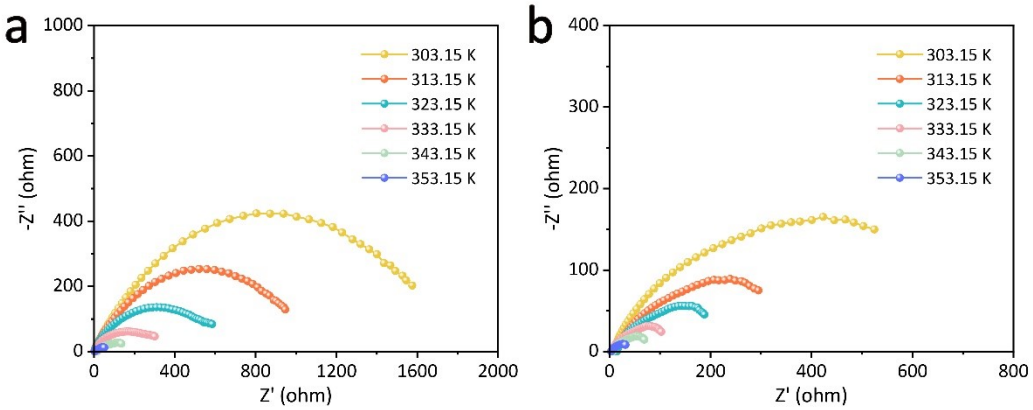

Figure S8. EIS of (a) bare Zn and (b) Zn@TOP/Carra electrodes at temperatures from 303.15 to 353.15 K.

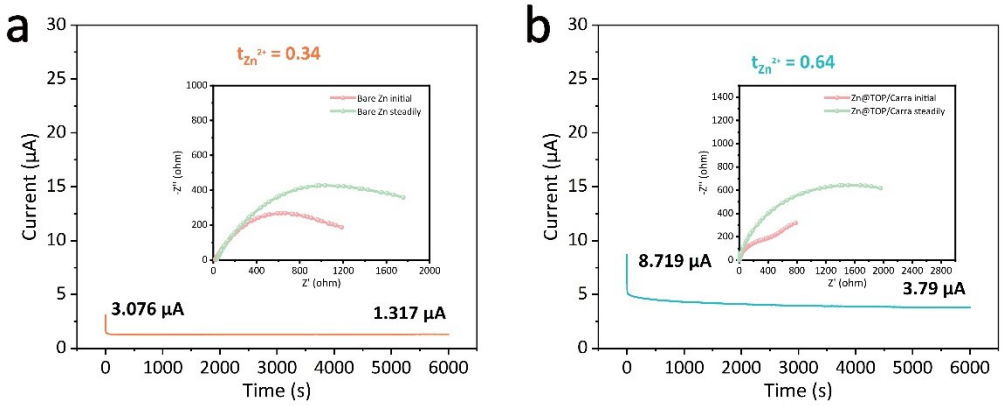

Figure S9. Chronoamperometry profiles and Nyquist plots of bare Zn and (b) Zn@TOP/Carra symmetric cells.

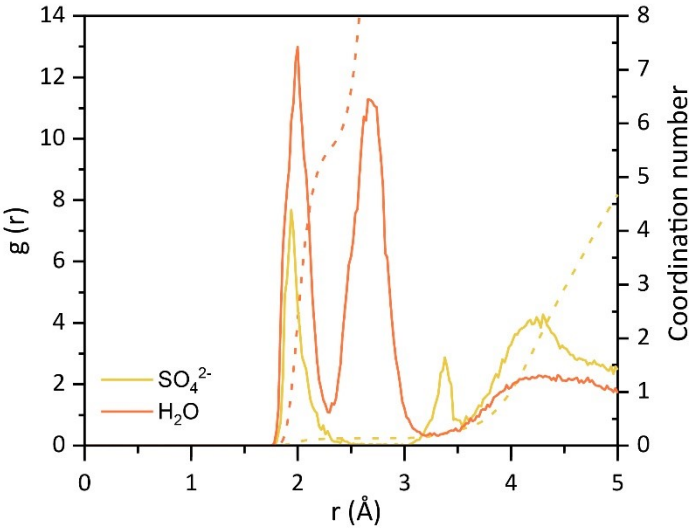

Figure S10. Coordination numbers (dash) and RDFs (solid) of Zn^{2+} solvation environment in bare Zn.

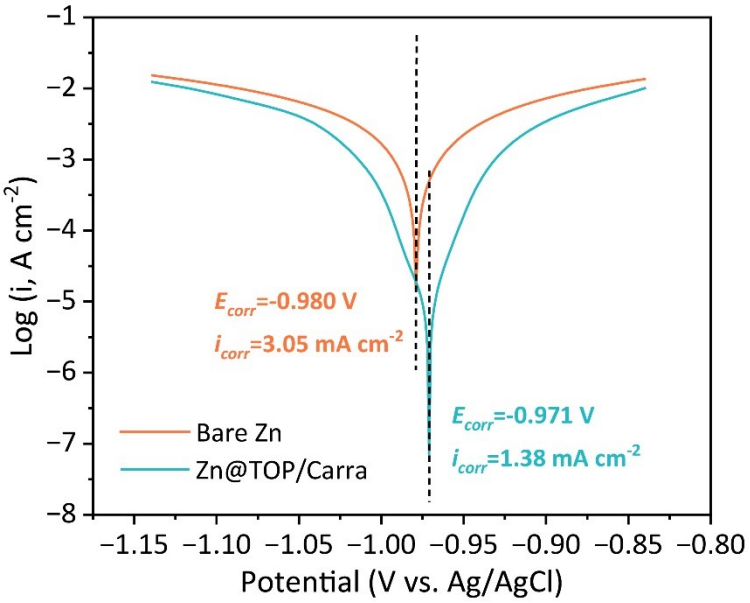

Figure S11. Corrosion curves of both bare Zn and Zn@TOP/Carra electrodes.

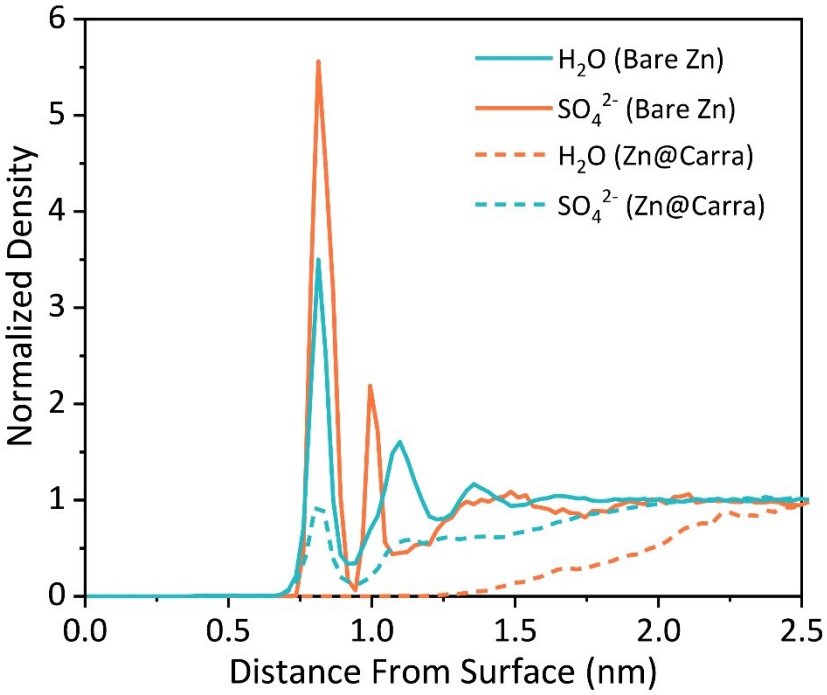

Figure S12. Normalized density profiles of both H_2O and SO_4^{2-} in the EDL of both bare Zn and Zn@Carra.

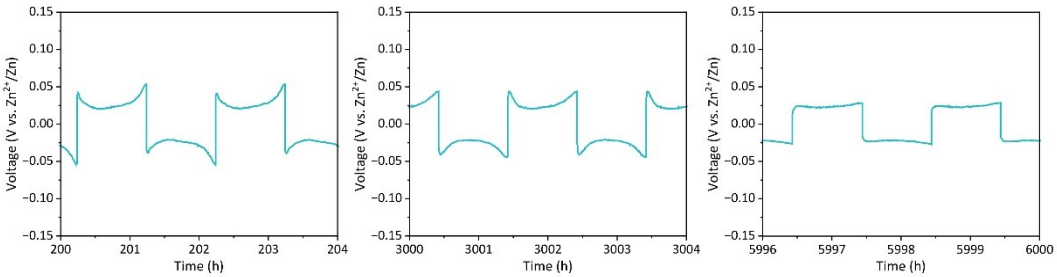

Figure S13. Enlarged voltage-time diagrams of the Zn@TOP/Carra||Zn@TOP/Carra symmetric cell at 1 mA cm^{-2} for 1 mAh cm^{-2}.

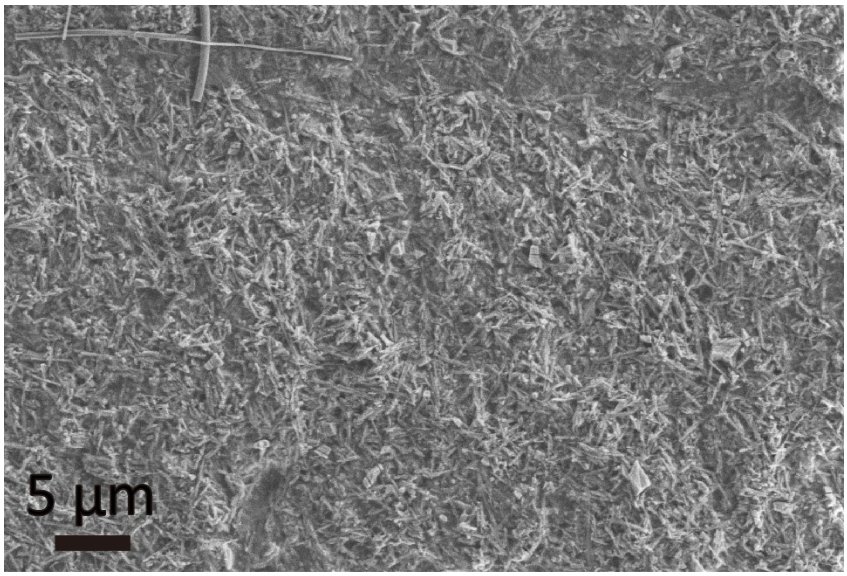

Figure S14. SEM image of the Zn@TOP/Carra electrode surface after 50 cycles.

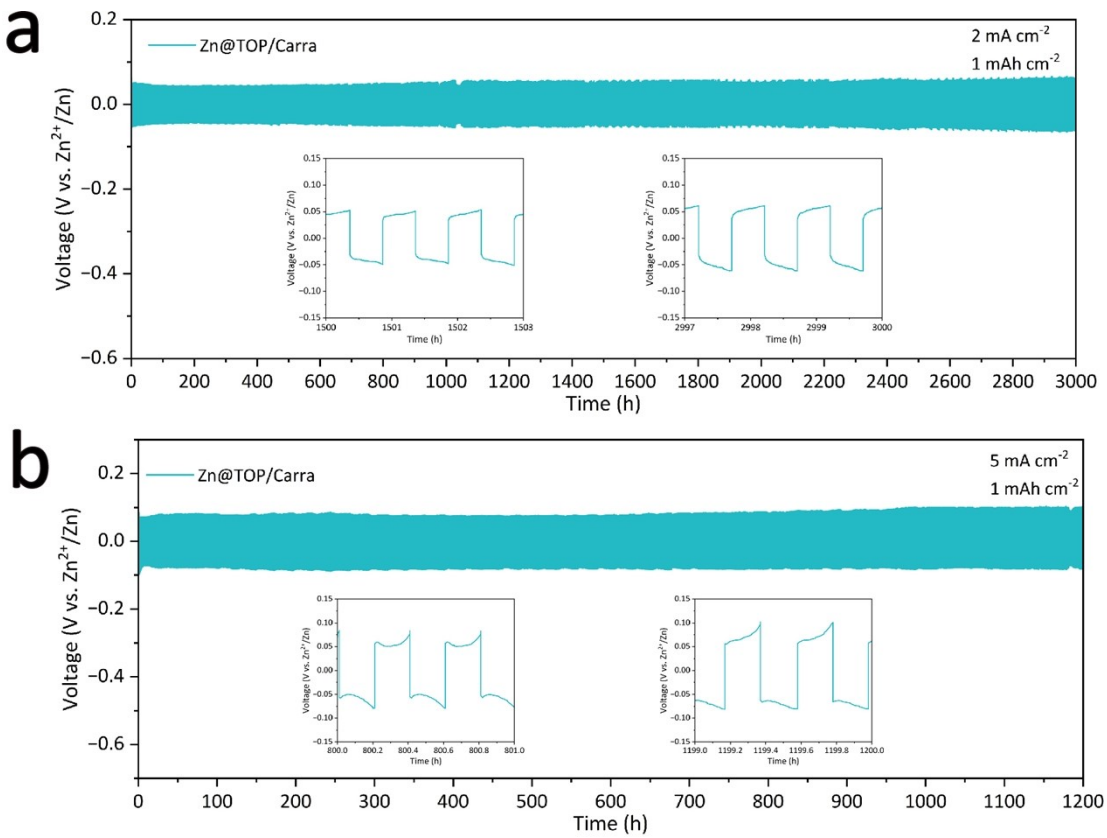

Figure S15. Time-voltage profiles of the Zn@TOP/Carra electrode (a) at 2 mA cm^{-2} for 1 mAh cm^{-2} and (b) at 5 mA cm^{-2} for 1 mAh cm^{-2}.

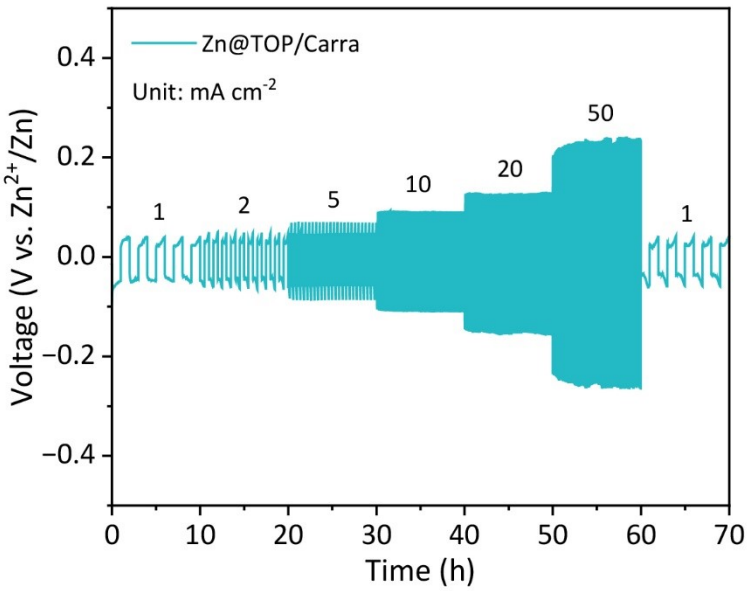

Figure S16. Rate capabilities of the Zn@TOP/Carra symmetric cell under different current densities of 1, 2, 5, 10, 20 and 50 mA cm^{-2}.

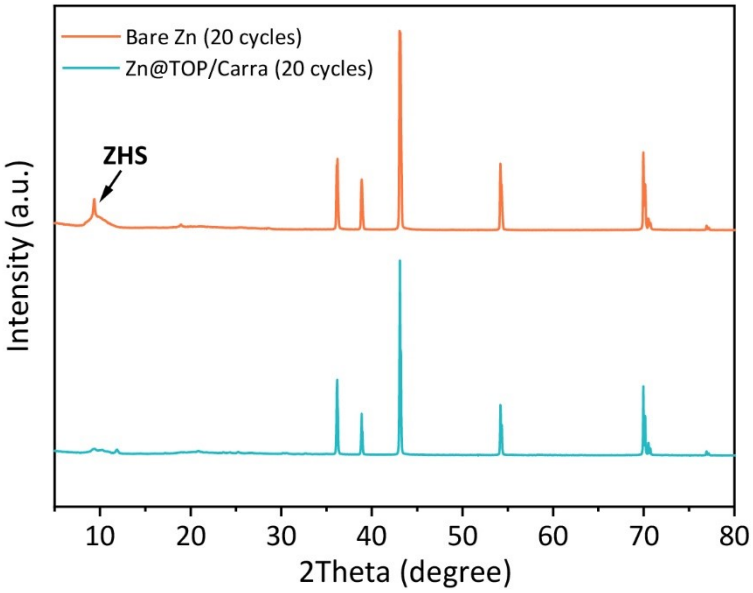

Figure S17. XRD patterns of both bare Zn and Zn@TOP/Carra electrodes after 20 cycles.

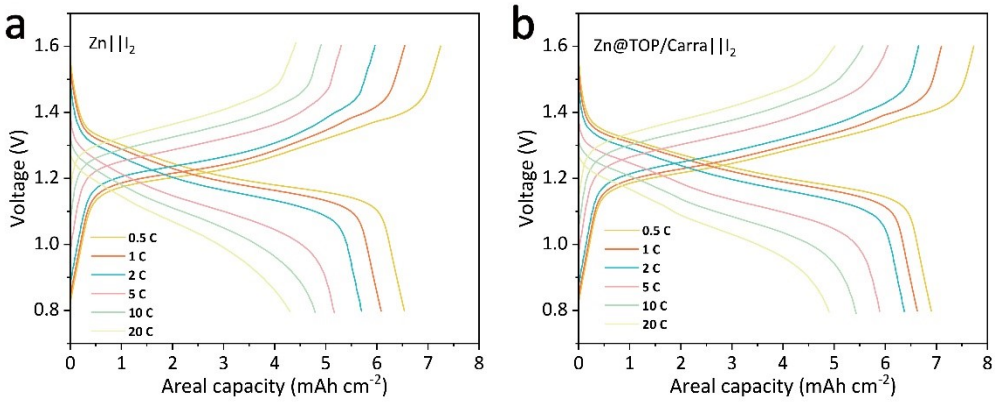

Figure S18. Capacity-Voltage profiles of (a) Zn||I_2 and (b) Zn@TOP/Carra||I_2 batteries at different cycling rates.

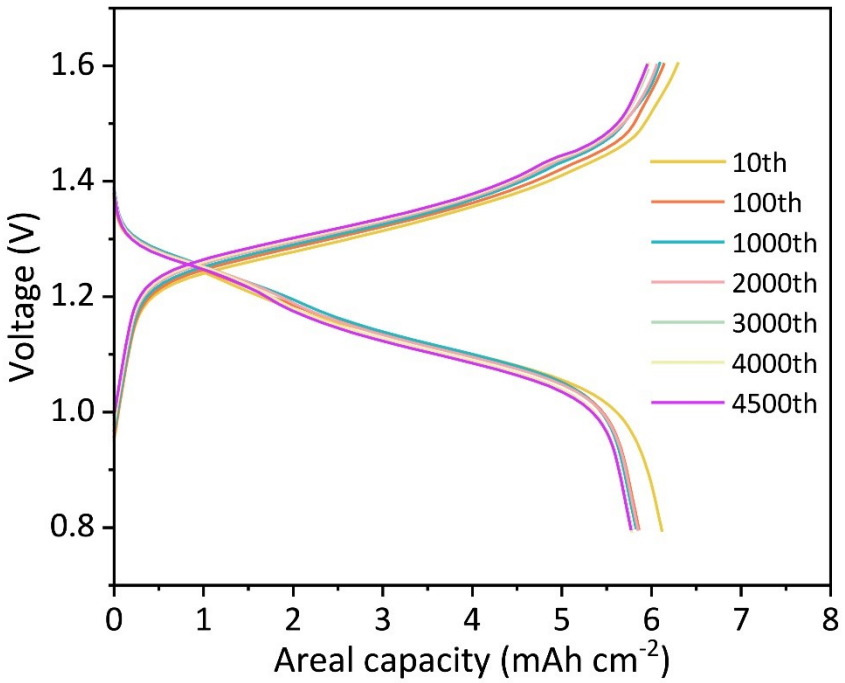

Figure S19. Capacity-Voltage profiles of Zn@TOP/Carra||I_2 battery cycling at 5 C.

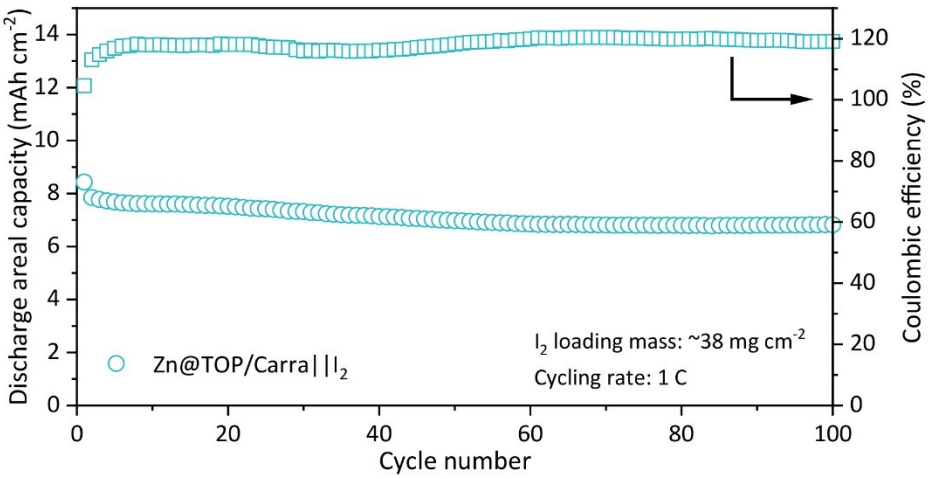

Figure S20. Cycling performance of the Zn@TOP/Carra||I_2 full battery at a relatively low cycling rate of 1 C.

References

[1] Deng, W.; Huang, Z.; Zhou, Z.; Li, C.; Chen, Y.; Zhou, Y.; Huang, C.; Zhu, J.; Zou, W.; Zhu, R.; Xu, Y.; Li, R. A Near 0 V and Low-Strain Intercalative Anode for Aqueous Zinc-Ion Batteries. *ACS Energy Lett.* **2023**, 3171–3179. https://doi.org/10.1021/acsenergylett.3c00985.

[2] Frisch, M. J.; Trucks, G. W.; Schlegel, H. B.; Scuseria, G. E.; Robb, M. A.; Cheeseman, J. R.; Scalmani, G.; Barone, V.; Mennucci, B.; Petersson, G. A.; et al. *Gaussian 09, Revision E.01*; Gaussian, Inc., Wallingford CT, 2013.

[3] Stephens, P. J.; Devlin, F. J.; Chabalowski, C. F.; Frisch, M. J. Ab Initio Calculation of Vibrational Absorption and Circular Dichroism Spectra Using Density Functional Force Fields. *J. Phys. Chem.* 1994, *98* (45), 11624-11627.

[4] Grimme, S.; Antony, J.; Ehrlich, S.; Krieg, H. A consistent and accurate ab initio parametrization of density functional dispersion correction (DFT-D) for the 94 elements H-Pu. *J. Chem. Phys.* 2010, *132* (15), 154104. DOI: 10.1063/1.3382344.

[5] Weigend, F.; Ahlrichs, R. Balanced basis sets of split valence, triple zeta valence and quadruple zeta valence quality for H to Rn: Design and assessment of accuracy. Phys Chem Chem Phys 2005, 7 (18), 3297-3305. DOI: 10.1039/b508541a.

[6] Weigend, F. Accurate Coulomb-fitting basis sets for H to Rn. Physical Chemistry Chemical Physics 2006, 8 (9). DOI: 10.1039/b515623h.

[7] A. V. Marenich, C. J. Cramer and D. G. Truhlar, *J. Phys. Chem. B*, 2009, 113, 6378.

[8] P. C. Christopher I. Bayly, and C. Wendy D, 5 and Peter A. Kollman*, J. Phys. Chem., 1993, 97, 10269.

[9] T. Lu and F. Chen, *J Comput. Chem.*, 33, 580.

[10] J. Zhang and T. Lu, *Phys. Chem. Chem. Phys.*, 2021, 23, 20323.

[11] M. J. Abraham, T. Murtola, R. Schulz, S. Páll, J. C. Smith, B. Hess and E. Lindahl, SoftwareX, 2015, 1-2, 19.

[12] H. J. C. Berendsen, J. R. Grigera and T. P. Straatsma, J. Phys. Chem., 1987, 91, 6269.

[13] K. Lindorff-Larsen, S. Piana, K. Palmo, P. Maragakis, J. L. Klepeis, R. O. Dror and D. E. Shaw, Proteins: Structure, Function, and Bioinformatics, 2010, 78, 1950.

[14] J. Wang, R. M. Wolf, J. W. Caldwell, P. A. Kollman and D. A. Case, J Comput. Chem., 2004, 25, 1157.

[15] A. W. S. d. Silva and W. F. Vranken, BMC Research Notes, 2012, 5, 367.

[16] Lu, T. Sobtop, Version [1.0], http://sobereva.com/soft/Sobtop: 2022.

[17] W. Kohn & L. J. Sham. Self-consistent equations including exchange and correlation effects. Phys. Rev. 140, A1133-A1138 (1965).

[18] A. Banerjee, N. Adams, J. Simons & R. Shepard. Search for stationary points on surfaces. J. Phys. Chem. 89, 52-57 (1985).

[19] L. Martínez, Andrade R A , Birgin E G ,et al.PACKMOL: A package for building initial configurations for molecular dynamics simulations[J].Journal of Computational Chemistry, 2010, 30(13):2157-2164.DOI:10.1002/jcc.21224.

[20] W. Humphrey, A. Dalke and K. Schulten, J. Mol. Graphics 1996, 14, 33.

[21] G. Kresse and J. Furthmuller, Phys Rev B, 1996, 54, 11169-11186.

[22] P. E. Blöchl, Phys. Rev. B 1994, 50, 17953.

[23] K. B. John P. Perdew, and Matthias Ernzerhof, Phys. Rev. Lett., 1996, 77, 3865.

[24] Hu, L.; Wu, Z.; Lu, C.; Ye, F.; Liu, Q.; Sun, Z. Principles of Interlayer-Spacing Regulation of Layered Vanadium Phosphates for Superior Zinc-Ion Batteries. *Energy Environ. Sci.* **2021**, *14* (7), 4095–4106. https://doi.org/10.1039/D1EE01158H.

[25] Zhang, Q.; Zhao, J.; Chen, X.; Yang, R.; Ying, T.; Cheng, C.; Liu, B.; Fan, J.; Li, S.; Zeng, Z. Unveiling the Energy Storage Mechanism of MnO_2 Polymorphs for Zinc-Manganese Dioxide Batteries. *Adv. Funct. Mater.* **2024**, 2306652. https://doi.org/10.1002/adfm.202306652.

[26] Liu, Y.; Lu, C.; Yang, Y.; Chen, W.; Ye, F.; Dong, H.; Wu, Y.; Ma, R.; Hu, L. Multiple Cations Nanoconfinement in Ultrathin V_2O_5 Nanosheets Enables Ultrafast Ion Diffusion Kinetics Toward High-performance Zinc Ion Battery. *Adv. Mater.* **2024**, *36* (18), 2312982. https://doi.org/10.1002/adma.202312982.

[27] Hu, L.; Wu, Z.; Lu, C.; Ye, F.; Liu, Q.; Sun, Z. Principles of Interlayer-Spacing Regulation of Layered Vanadium Phosphates for Superior Zinc-Ion Batteries. *Energy Environ. Sci.* **2021**, 10.1039.D1EE01158H. https://doi.org/10.1039/D1EE01158H.